

S1. Satellite imagery, electrical resistivity tomography, stratigraphy, pedology

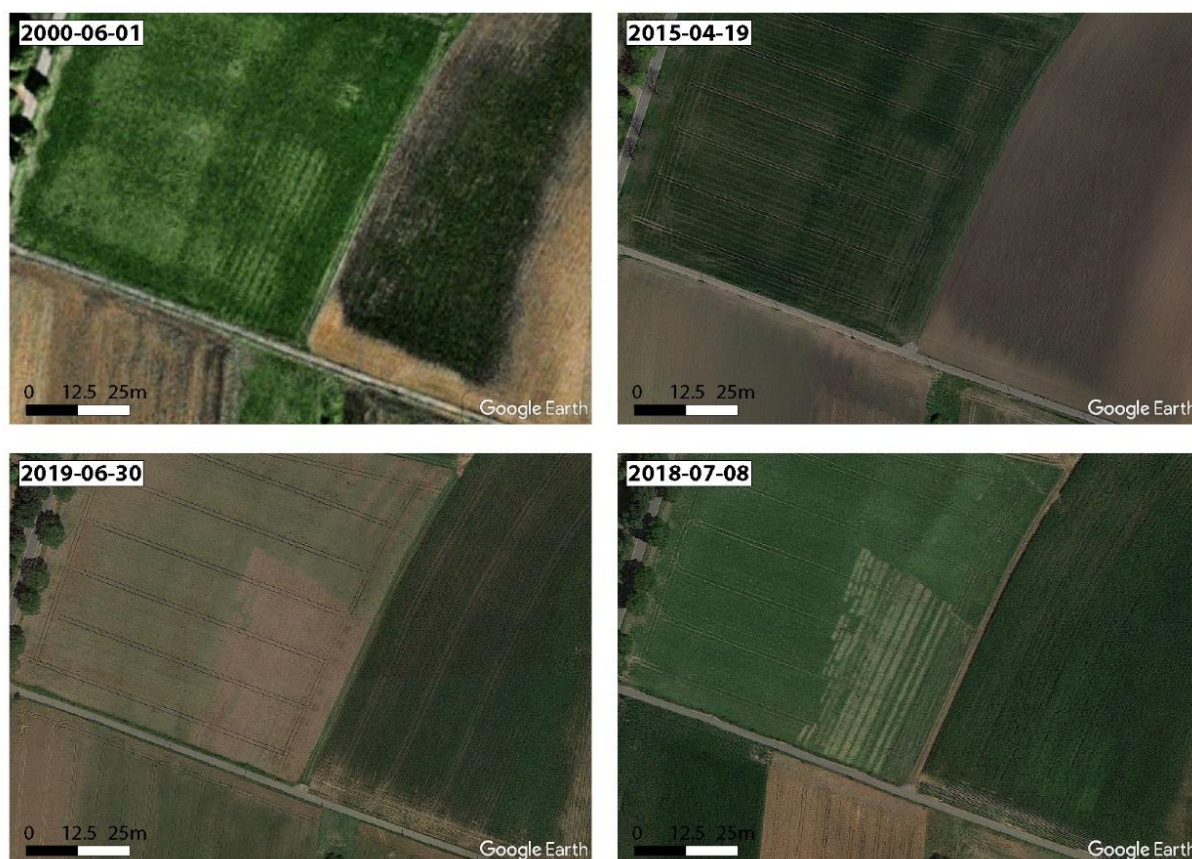


Figure S1. Satellite images indicating the linear anomalies in the spring and summer seasons (map data: Google ©2025 GeoContent, Landsat/Copernicus, all accessed through Google Earth Pro).

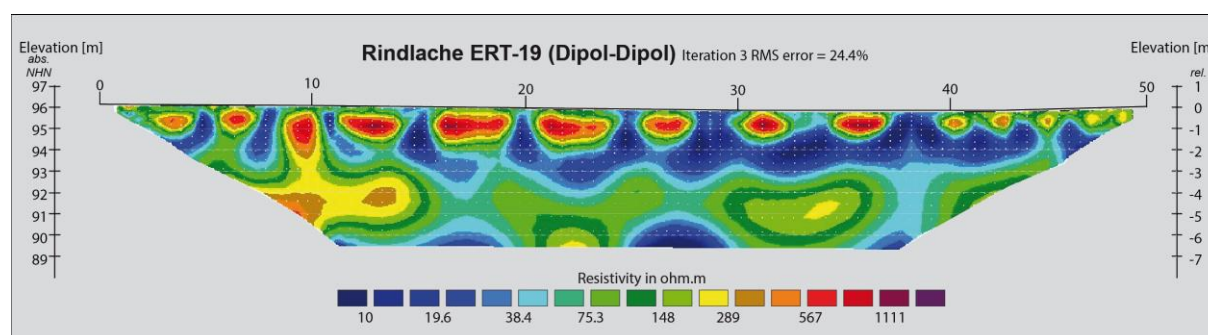


Figure S2. Electrical resistivity topography transect across the linear anomaly in Dipol-Dipol configuration. For location see Fig. 2A; for Schlumberger configuration of the same transect see Fig. 2D.



Figure S3. Mudrape and mudclasts from the sand infill of Pit 2.



Figure S4. Larger mudclast from the sand in fill of Pit 2.



Figure S5. Section of sand infill overlain by Unit S1 in Pit 1, view towards the south. Excessive, localised carbonate precipitation in S1 results from anthropogenic amelioration after infilling the trenches with sand.



Figure S6. Hollow brick in the light-coloured sand infill left by the land consolidation campaign Viernheim DF 459 from the 1970/80s.



Figure S7. Unit S3 in Pit 2, vertically confined by discontinuous light-coloured sand of units S2 and S4. The sand units show sharp, irregular boundaries with signs of bioturbation.



Figure S8. Unit S6 in Pit 2, characterised by excessive carbonate precipitation (*Rheinweiß*), overlain by the brown fossil top soil of Unit S5.

Table S1: Soil horizons associated with the stratigraphic units of Pit 2 (Fig. 3, main text), according to KA6 (Ad-hoc AG Boden, 2024) and KA5 (Ad-hoc AG Boden, 2005).

Unit	KA6	KA5	Description
S1	Dj	jC	Mineral subsoil horizon originating from nature-based anthropogenic infill (i.e., sand in the present case)
S2	Dj	jC	
S3	Dj	jC	
S4	Dj	jC	
S5	Gor - eMm	Gor - aeM	Holocene floodplain-borne soil sediment with marly texture and influence of groundwater level fluctuations; predominantly reducing conditions throughout the year
S6	Gor - eMcm	Gor - aeMc	Holocene floodplain-borne soil sediment with marly texture, influence of groundwater level fluctuations and secondary precipitation of carbonates (predominantly reducing conditions throughout the year)
S7	eMm	aeM	Holocene floodplain-borne soil sediment with marly texture
S8	eMm	aeM	
S9	fnH	fnH	Fossil organic (≥ 30 vol. %) horizon originating from fen peat vegetation
S10	feF °Gor	feF °Gor	Fossil, marly subhydric horizon under the influence of later groundwater level fluctuations (predominantly reducing conditions throughout the year) → gyttja

S2. Historical documents

Transcription of the original text (cf. Fig. S9) in kurrent script into modern German:

„Situations-Plan

Über die Anlage einer Feldbacksteinbrennerei des Ackermann Peter Minnig in Viernheim

Nr. 2 = Acker des Großherzoglichen Bürgermeisters Michael Keller (1862–1873)

Nr. 1 = 1359 Klafter

Nr. 3 = 1473 Klafter – Acker des Peter Minnig

Der Acker Nr. 1 ist das Grundstück auf welchem die Feldbacksteinbrennerei angelegt werden soll. Derselbe liegt 1/2 Stund in südlicher Richtung von Viernheim und ist 450 Fuß breit und 360 Fuß lang. Die Erd zur Backsteinfabrikation wird in der Mitte des Grundstücks gegraben und die Gruben sogleich wieder ausgefüllt. Die Backsteine werden von Zeit zu Zeit ohngefähr in der Mitte des Grundstücks zusammengesetzt und mit Steinkohlen gebrannt. Viernheim den 1ten Juni 1865 PMinnig”

English translation:

“Situation plan

On the construction of a brickworks site of the farmer Peter Minnig in Viernheim

No. 2 = field of the mayor Michael Keller

No. 1 = 1359 fathoms

No. 3 = 1473 fathoms – field of Peter Minnig

Field no. 1 is the plot on which the brickworks site shall be established. The plot is situated ½ hour south of Viernheim, and it is 450 feet wide and 360 feet long. The substrate for the brick manufacture will be excavated in the center of the plot and the pits will be refilled immediately. From time to time the bricks are put together approximately in the center of the plot and burnt with stone coal. Viernheim 1st June 1865 PMinnig”

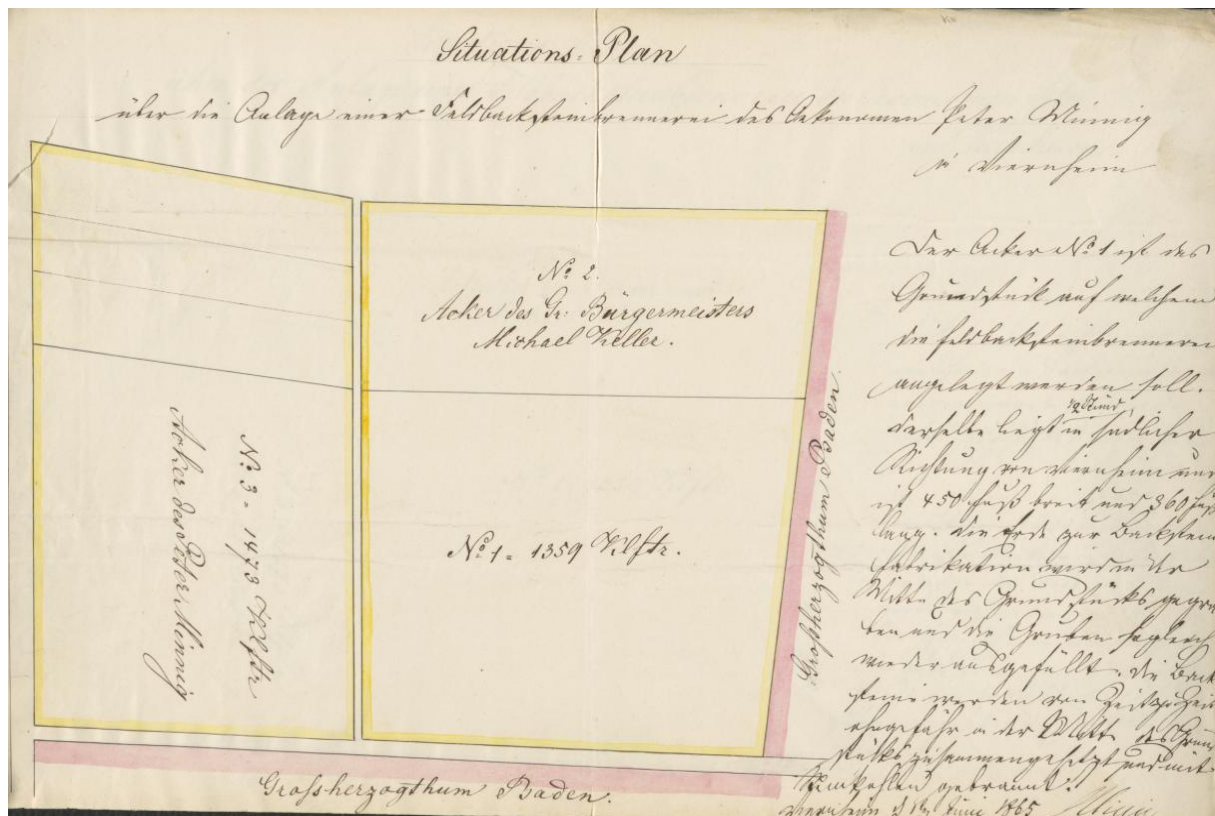


Figure S9. Localization of the brickyard of Peter Minnig, licensed in AD 1865. Plan appended to the license for the brickyard (digital version, image 90).

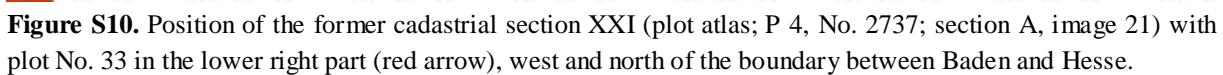


Figure S10. Position of the former cadastral section XXI (plot atlas; P 4, No. 2737; section A, image 21) with plot No. 33 in the lower right part (red arrow), west and north of the boundary between Baden and Hesse.

S3. OSL sampling and sample preparation

Sampling

From each of the two pits – Pit 1 and Pit 2, see Fig. 2A and result section of the main text – three samples were taken for optically stimulated luminescence (OSL) dating (for details on the method cf. Aitken 1985, 1998) in the light-coloured sand infill. The OSL samples were collected in light-proof steel cylinders (\varnothing 4.7 cm x 30 cm, for sample OSL-4; \varnothing 7.2 cm x 9 cm for all other samples) hammered horizontally into the cleaned pit walls (Figs. S11, S12; Table S2). Sample preparation occurred under strongly dimmed indirect red light in the Heidelberg Luminescence Laboratory. The outer, possibly light-contaminated sample parts were eliminated in the dark lab and retained for dose rate determination. The samples water content was determined gravimetrically by weighing the samples immediately after unpacking them from the steel cylinders (sample's wet weight), and after drying the samples at 50 °C, until after repeated weighing no further weight loss was observed (sample's dry weight).

Table S2. OSL samples from Pit 1 (SW; 8.58125 °E, 49.520309 °N, 95.9 m above sea level [a.s.l.]) and Pit 2 (NE; 8.581431 °E, 49.520605 °N, 95.7 m a.s.l.); b.s. = below surface.

Pit	Field code	Lab. code	Depth b.s. [cm]
1	OSL-6	HDS-1823	75
1	OSL-5	HDS-1822	95
1	OSL-4	HDS-1821	113
2	OSL-3	HDS-1820	63
2	OSL-2	HDS-1819	100
2	OSL-1	HDS-1818	132



Figure S11. View from southwest onto the northeastern wall of Pit 1 with the position of OSL samples 4–6 (HDS-1821 to HDS-1823) taken in the sand infill.



Figure S12. OSL samples 1–3 (HDS-1818 to HDS-1820) from the sand infill of Pit 2.

Selection of appropriate mineral separates

Under light influence the latent luminescence signal of quartz is reset more rapidly and more thoroughly compared to feldspar, i.e., quartz bleaches faster than feldspar (Godfrey-Smith et al., 1988). Following the working hypothesis that sand had been taken from the nearby Bettenberg dune, carried to nowadays' parcel No. 153 to fill up the trenches resulting from clay mining by using shovels and barrows only, the possibility for a resetting of the luminescence signal was considered minimal. The material was likely

filled in as shovelled lumps and not as individual mineral grains (as e.g., during aeolian sand transport). Therefore, quartz coarse grains (125–212 μm) were extracted from the OSL samples following standard procedures (see workflow in Fig. S13). For OSL measurements the extracted quartz separates were placed as a single-layer on aluminium cups (\varnothing 10 mm, 1 mm thick) through a hole mask (\varnothing 4 mm) preparing „small aliquots“ (10^2 grains each aliquot). Mineral grains were fixed on the sample carriers using silicon spray.

Sampling in the field	
	<ul style="list-style-type: none"> Collect samples in opaque metal cylinders, metal boxes, PE liner-tubes or similar Carve out larger blocks (dried/hardened sediment only)
Sample preparation in the luminescence laboratory under strongly subdued red light	
[1]	<ul style="list-style-type: none"> Eliminate outer, potentially light affected sample rims <ul style="list-style-type: none"> Retain not light-affected sample for luminescence dating (1) Retain outer sample rims for dose rate determination (2) (not further considered in this work flow)
[2]	<ul style="list-style-type: none"> Use (1) and determine sample's wet weight Use (1) and dry at 50 °C; weigh repeatedly until no further loss of weight is observed (3) Determine sample's water content (wet weight : dry weight; needed for dose rate determination)
[3]	<p>Only if there is a surplus of fine-grained material (silt, clay) and little coarse-grained material (fine sand)</p> <ul style="list-style-type: none"> Use dried inner sample part (3) and dilute in aqua_{demin}; separate muddy components (3a) from coarser components (3b); proceed with steps [4]–[7] on the two fractions (3a) and (3b) separately Proceed with dried inner sample part (3); or with subfractions (3a) and (3b), respectively
[4]	<ul style="list-style-type: none"> Eliminate carbonate content with acetic acid (CH_3COOH; 20 %); rinse with aqua_{demin} (4)
[5]	<ul style="list-style-type: none"> Eliminate organic content with hydrogen peroxide H_2O_2 (10 % and 30 %); rinse with aqua_{demin} (5)
[6]	<ul style="list-style-type: none"> Disperse sample (5) with sodium oxalate ($\text{Na}_2\text{C}_2\text{O}_4$, 0.01 N); rinse with aqua_{demin} (6)
[7]	<ul style="list-style-type: none"> Sieve sample (6) <ul style="list-style-type: none"> For coarse grains with mesh sizes of 212 μm and 125 μm; retain fraction < 125 μm (7); retain fraction 125–212 μm (8) For fine grains use fraction < 125 μm (7); sieve with mesh size 63 μm; retain fraction < 63 μm (9)
	<ul style="list-style-type: none"> Extract polymineral fine grains (4–11 μm)
[8]	<ul style="list-style-type: none"> Use fraction < 63 μm (9); separate fraction < 11 μm in aqua_{demin} (beaker or Atterberg cylinder); retain fraction < 11 μm (10)
[9]	<ul style="list-style-type: none"> Use fraction < 11 μm (10); remove fraction < 4 μm in aqua_{demin} (centrifuge); retain resulting mineral separate 4–11 μm as polymineral fine grains (4–11 μm) (11)
	<ul style="list-style-type: none"> Extract quartz fine grains (4–11 μm)
[10]	<ul style="list-style-type: none"> Use polymineral fine grains (11); etch in fluorosilicic acid ($\text{H}_2[\text{SiF}_6]$; 35 %) for 5 days in PET beaker (sample : acid = 1 : 4); swirl beaker once every workday; rinse with aqua_{demin} (5 times)
[11]	<ul style="list-style-type: none"> Remove fluorides with hydrochloric acid (HCl, 10 %) over night; stir 3 times (usually 2 times first day, 1 time second day); rinse with aqua_{demin} (until pH = 7); retain resulting mineral separate as quartz fine grains (4–11 μm) (12)
	<ul style="list-style-type: none"> Extract quartz coarse grains (125–212 μm)
[12]	<ul style="list-style-type: none"> Use fraction 125–212 μm (8); remove heavy minerals (fraction > 2.74 g/cm³) in lithium polytungstate (LST, 2.74 g/cm³); retain fraction < 2.74 g/cm³ (13)
[13]	<ul style="list-style-type: none"> use fraction < 2.74 g/cm³ (13) to separate lighter minerals < 2.64 g/cm³ from heavier minerals > 2.64 g/cm³ in LST (2.64 g/cm³); retain fraction 2.64–2.74 g/cm³ (14) and fraction < 2.64 g/cm³ (15) (the latter for feldspar preparation)
[14]	<ul style="list-style-type: none"> Use fraction 2.64–2.74 g/cm³ (14); etch in hydrofluoric acid (48 %; magnetic stirrer on low level) for 45 min in teflon beaker; rinse with aqua_{demin} (5 times)
[15]	<ul style="list-style-type: none"> Remove fluorides with hydrochloric acid (HCl, 10 %) over night; rinse with aqua_{demin} (until pH = 7); retain resulting mineral separate as quartz coarse grains (125–212 μm) (16)

Figure S13. Schematic work flow of sample preparation at heiLUM. Work steps for sample collection and extracting quartz coarse grains as applied in the present study are highlighted in green (from Pfaffner et al., 2025, Fig. S2.2.1; slightly modified).

Instrumentation

The quartz coarse grain extracts were analysed with a blue-light stimulated luminescence (BLSL) single aliquot regeneration (SAR) protocol (Murray and Wintle, 2003) on a luminescence reader model Risø DA15 (Bøtter-Jensen et al., 2000), updated to DA20 (DTU Physics, 2021), which is equipped as shown in Fig. S14.

Luminescence reader: Risø model TL/OSL DA15, upgraded DA20 (No. 83)				
turntable: 48 measurement positions				
use every 2 nd position (or wider spacing) to avoid IR cross talk (ignore for this study)				
IR stimulation: bleaching of IR ₁₂₅ signal from feldspar prior to BLSL ₁₂₅ signal detection				
IR-LEDs; 3 clusters; 7 LEDs each; 870 Δ 40 nm				
measurements with 90 % diode-power, after 10 s warmup				
Blue light stimulation: detection of BLSL ₁₂₅ signal assumed to originate (mostly) from quartz				
blue light emitting diodes; four clusters; 7 LEDs each; 470 Δ 30 nm				
measurements with 90 % diode-power, after 10 s warmup				
Detection: bialkali PMT EMI 9235QB15				
Detection filter: U340 (Schott; 3 x 2.5 mm thick)				
Detected emission: violet, around 340 nm				
β-dose rate:	0.05785 ± 0.00185	Gy/s	21. October 2021	(start this study)
	3.47 ± 0.11	Gy/min		
	0.05664 ± 0.00181	Gy/s	07. September 2022	(end this study)
	3.40 ± 0.11	Gy/min		
Nitrogen use: ca. 4 minutes at start of measurement				

Figure S14. Equipment of the luminescence reader model Risø DA15, updated to DA20, used for the BLSL SAR measurements of the quartz coarse grains (125–212 μm).

Test on the palaeodose range – equivalent dose (De) range test

In OSL dating, the palaeodose a sample has acquired since the last being reworked is proxied by the size of its natural luminescence signal. The natural luminescence signal is compared to a laboratory dose (equivalent dose; De) which induces an equally strong luminescence signal as the natural palaeodose. In a first test for adapting the BLSL SAR protocol to the samples of this study, the natural dose of the three samples HDS-1821 to HDS-1823 from Pit 1 was checked with a not yet optimized SAR protocol to receive an idea of the expected range of the palaeodoses. In contrast to the finally adapted SAR protocol (Fig. S14), the protocol applied to the De range test used a temperature of 180 °C for 10 s for preheat 1 and 160 °C for 10 s for preheat 2, and a normalisation dose (also „test dose“) of 40 s beta irradiation time, corresponding to ca 2.27 Gy on reader No. 83 at the time of measurement. BLSL stimulation occurred at 125 °C (BLSL₁₂₅). OSL stimulation occurred for 40 s using 250 data channels (0.16 s per data channel).

De determination for this test and all other measurements was performed with the software Luminescence Analyst, version 4.31.9 (Duller, 2015). Due to the poor data quality, no quality criteria were applied for accepting or rejecting aliquots for the De range test. The results of the test show a wide range of De values from ca. 0.5 Gy to 15 Gy (Table S3). But most aliquots point to comparatively high palaeodoses which do not seem to represent bleaching in the recent past.

Table S3. De range test on samples HDS-1821 to HDS-1823 (two aliquots each) with a not yet optimized BLSL SAR protocol. De integral 0–0.64 s, integral for late light subtraction 30.1–40 s. Exponential plus linear fit.

Sample [HDS-no.]	Aliquot [#]	De [s]	[ca. Gy]		
HDS-1821	1	261.42	± 15.09	15.1	
HDS-1821	2	111.75	± 20.99	6.5	
HDS-1822	1	157.02	± 22.43	9.1	
HDS-1822	2	8.66	± 3.30	0.5	
HDS-1823	1	128.61	± 7.53	7.4	
HDS-1823	2	193.31	± 10.51	11.2	

A second De test on all six OSL samples (8 aliquots each) was performed after also samples HDS-1821 to HDS-1822 had been prepared. Again, a similarly large De scatter was observed for each sample, and none of the samples could be chosen as the probably best bleached sample for the dating measurements. Again, quality criteria for accepting aliquots did not apply, as otherwise (almost) no Des had been determinable. Many aliquots were rather dim or showed background light.

Test on the luminescence signal strength

In a further test the brightness of differently sized aliquots was investigated. Besides the „small“ aliquots (10^2 grains) we also tested so called „tiny“ aliquots (10^1 grains) and „supertiny“ aliquots (10^0 grains) of samples HDS-1821 to HDS-1822. This test was performed because not-properly-bleached samples are best investigated with aliquots with low grain numbers, as these might comprise some aliquots which may consist only of the best bleached grains. However, this approach did not provide any better results either.

Combined preheat and dose recovery test

We performed a combined preheat and dose recovery test on 48 small aliquots of sample HDS-1820. First, the aliquots were bleached under a solar simulator type SOL 2 (Hönle) for 3 h. During bleaching the sample holder was covered with a UVILEV filter glass to align the light to the solar spectrum and placed on a water-cooled copper plate (ca 22 °C) to avoid heating of the aliquots under the glass cover. Afterwards, the aliquots were stored for at least 24 h at room temperature in the dark to allow potential charge transfer to decline prior to BLSL SAR measurement.

In order to improve the luminescence count statistics, the normalisation dose was increased to 100 s beta-irradiation time (ca 5.7 Gy) and the laboratory dose was set to 300 s (ca. 17 Gy). The BLSL SAR dose response curve was build up with regeneration dose points as follows: 30 s (ca 1.7 Gy; 10 % of the expected dose), 120 s (6.8 Gy; 40 %), 210 s (11.9 Gy; 70 %), 300 s (17 Gy; 100 %), 390 s (22.2 Gy; 130 %), 480 s (27.3 Gy; 160 %), 0 s (0 Gy; 0 %; to test signal recuperation by the preheating procedure), 120 s (6.8 Gy; 40 %; to test the reproducibility of a repeatedly administered dose; recycling ratio) and 300 s (17 Gy; 100 %; the dose point is read out by BLSL after IR-stimulation to test the OSL IR depletion ratio as a proxy for feldspar contamination, cf. Duller, 2003). The preheat procedures lasted always for 10 s. We set preheat 1 to 160 °C and increased preheat 2 from 160 °C to 260 °C, in steps of $\Delta 20$ °C, using 8 aliquots per group. BLSL readout occurred at 125 °C for 40 s (400 data channels; 0.1 s per data

channel). Only the preliminary De tests were carried out with 250 data channels for 40 s OSL readout (0.16 s per data channel), whereas the dose recovery tests and the De measurements were performed with 400 data channels for 40 s OSL readout (0.1 s per data channel).

The dose response curve was modelled with an exponential plus linear fit. De determination occurred on the first four data channels (0–0.4 s) using the channels 301–400 (30.1–40 s) for late light subtraction. An example of a measured aliquot is given in Fig. S15, Table S4.

As a result of the combined preheat and dose recovery test, 31 out of 48 measured aliquots were analysable when applying the following quality criteria for accepting aliquots: recycling ratio, maximum test dose error, and recuperation $\leq 10\%$ and normalisation dose signal > 3 sigma above the background, showing that increasing the normalisation dose efficiently improved the data quality (Figs. S16–S18). Almost all recovered Des meet the expected dose within 10 % error margins. A preheat-1 temperature $\geq 200\text{ }^{\circ}\text{C}$ leads to recycling ratios and recuperation values often at the limit or beyond the accepted range of deviation from the optimal value (zero for recuperation; 1 for the recycling ratio). The comparably mildest preheat procedure, with preheat-1 and preheat-2 both at $160\text{ }^{\circ}\text{C}$, appears to be best suited for the samples of this study. For this preheat group of aliquots all aliquots proved analysable, giving an unweighted mean with standard deviation and standard error of $299.6\text{ s} \pm 22.1\text{ s} \pm 7.8\text{ s}$ and a central dose of $298.5\text{ s} \pm 5.0\text{ s}$ (for details of the central age model, CAM, cf. Galbraith et al., 1999), with both values reproducing the expected value well.

We also tested the shorter De interval of channel 1 (0–0.1 s) with the same integral for background subtraction (channel 301–400; 30.1–40 s). No systematic differences to the De integral 0–0.4 s were observed (Fig. S15, Table S4). Therefore, for the dating measurements the slightly longer De interval was preferred, because of the better luminescence count statistics.

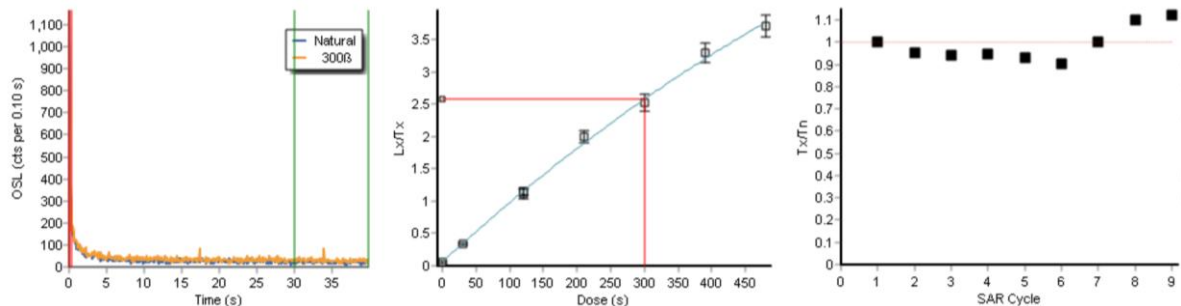


Figure S15. Example of shine down curve (left), dose response curve (center) and the sensitivity changes of the normalisation dose during a complete BLSL SAR run (here T_x/T_n over SAR cycle) (right) of aliquot 6 (preheat $160\text{ }^{\circ}\text{C}/160\text{ }^{\circ}\text{C}$) of the combined preheat and dose recovery test on artificially bleached and dosed small aliquots of sample HDS-1820. Dose response curve modelled with an exponential plus linear fit. De integral 0–0.1 s, integral for late light subtraction 30.1–40 s. Graphical output from the software Luminescence Analyst, version 4.31.9 (Duller, 2015).

Table S4. Recovered De values (s irradiation time) in alternating blue and green colour denoting the different groups of preheat temperatures (8 aliquots per group). The two different De intervals 0–0.1 s and 0–0.4 s deliver the same results within error margins and no systematic difference between the shorter and the longer De interval is observed. This is in contrast to most of the natural Des (cf. Figs. S20–S27, Tables S5–S12).

turntable position [#]	aliquot [#]	determined dose [s irradiation time] [0 - 0.1 s]		determined dose [s irradiation time] [0 - 0.4 s]		Diff long vs. short De interval [s irradiation time] [0 - 0.4 s] - [0 - 0.1 s]
1	1	322.25	35.52	338.52	24.08	16.27
2	2	302.53	19.11	298.94	15.35	-3.59
3	3	241.66	32.15	261.50	21.85	19.84
4	4	302.08	11.87	290.85	9.15	-11.23
5	5	289.97	18.36	307.10	16.43	17.13
6	6	296.25	22.09	300.53	16.92	4.28
7	7	313.31	14.59	312.39	12.19	-0.92
8	8	291.32	15.13	286.58	12.06	-4.74
9	9	n.a.		349.35	34.55	
10	10	285.76	29.20	292.69	22.80	6.93
11	11	n.a.		n.a.		
12	12	n.a.		n.a.		
13	13	331.59	17.47	329.26	15.67	-2.33
14	14	277.03	16.00	278.45	12.70	1.42
15	15	274.13	14.89	n.a.		
16	16	328.76	10.03	326.30	9.24	-2.46
17	17	n.a.		n.a.		
18	18	275.47	31.45	282.33	25.46	6.86
19	19	267.03	32.45	n.a.		
20	20	n.a.		n.a.		
21	21	295.93	17.60	296.29	13.72	0.36
22	22	n.a.		n.a.		
23	23	331.56	33.04	327.21	25.30	-4.35
24	24	298.10	18.62	288.49	14.30	-9.61
25	25	252.64	12.57	249.10	10.70	-3.54
26	26	350.67	45.16	n.a.		
27	27	266.61	22.99	271.10	17.07	4.49
28	28	280.92	15.14	298.33	13.06	17.41
29	29	277.01	38.27	274.98	24.45	-2.03
30	30	288.42	11.84	290.45	10.36	2.03
31	31	n.a.		n.a.		
32	32	294.27	19.59	279.68	15.05	-14.59
33	33	264.05	20.50	254.07	14.12	-9.98
34	34	254.79	17.18	261.10	14.22	6.31
35	35	378.38	34.02	n.a.		
36	36	n.a.		n.a.		
37	37	351.19	26.96	n.a.		
38	38	314.27	19.63	296.40	15.21	-17.87
39	39	n.a.		n.a.		
40	40	281.38	23.67	n.a.		
41	41	292.51	23.39	299.25	18.73	6.74
42	42	305.34	22.70	295.34	18.67	-10.00
43	43	439.38		n.a.		
44	44	225.38	29.52	n.a.		
45	45	n.a.		318.21	29.94	
46	46	214.70	15.03	233.64	13.48	18.94
47	47	n.a.		262.49	27.65	
48	48	n.a.		n.a.		

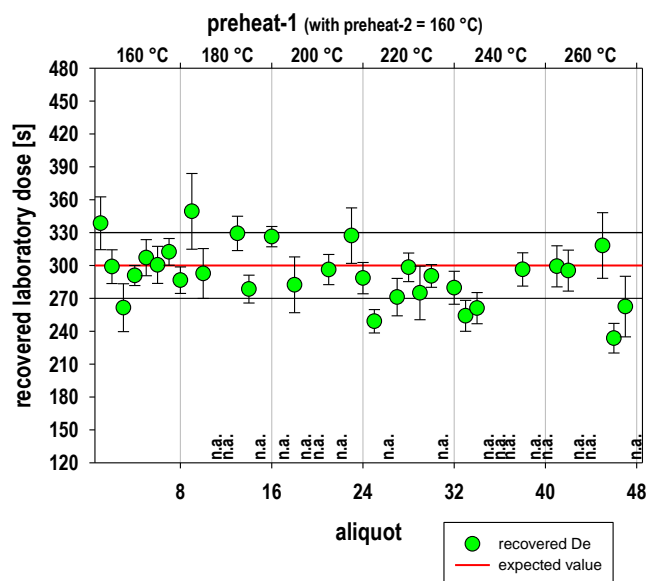


Figure S16. Results of the combined preheat and dose recovery test on small aliquots of sample HDS-1820. Administered dose 300 s (17 Gy); normalisation dose 100 s (5.7 Gy): Recovered doses.

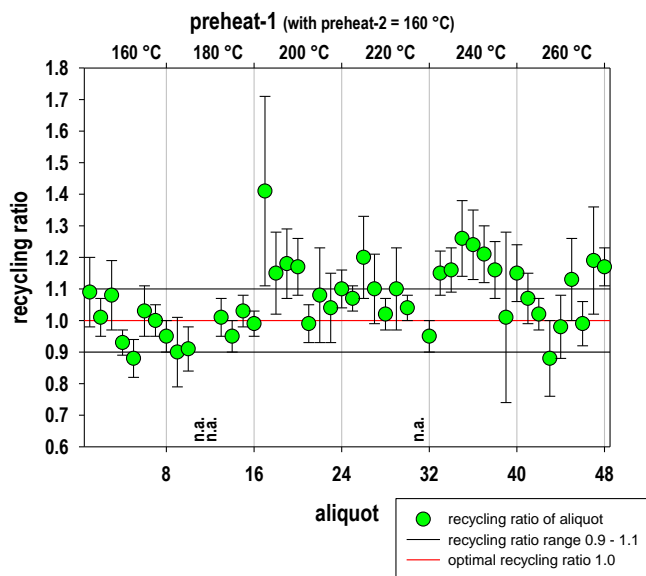


Figure S17. Results of the combined preheat and dose recovery test on small aliquots of sample HDS-1820. Administered dose 300 s (17 Gy); normalisation dose 100 s (5.7 Gy): Recycling ratios.

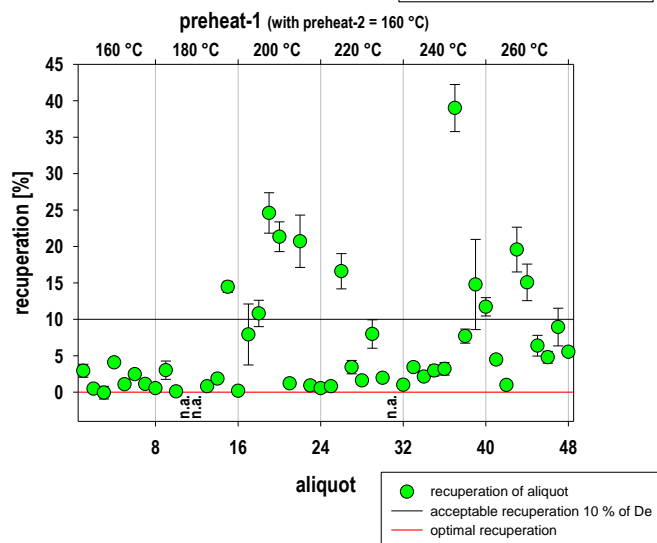


Figure S18. Results of the combined preheat and dose recovery test on small aliquots of sample HDS-1820. Administered dose 300 s (17 Gy); normalisation dose 100 s (5.7 Gy): Recuperation as percentage of the recovered De. The red lines denote the optimal values, the black lines the 10 % range of the optimal values.

Testing tiny aliquots with the 300 s dose response curve and a normalisation dose of 100 s

We also tested whether the use of „tiny“ aliquots (10^1 grains) was possible when applying the BLSL₁₂₅ SAR protocol with the 300 s dose response curve (300 s corresponding to the expected dose, i.e., 100 % ca. 17 Gy) and the larger normalisation dose of 100 s (ca. 5.7 Gy). Yet, when applying the data quality criteria as for the dose recovery test on the small aliquots, only four out of 48 measured aliquots were analysable. Apparently, the quartz coarse grains from the sand infill of the trenches are too dim, or too few grains are bright enough, to measure aliquots with only very few grains (Figs. S16–S18).

BLSL SAR protocol

Based on the results of the pre-tests, the BLSL SAR dating measurements were performed on small aliquots (10^2 grains) (Fig. S19).

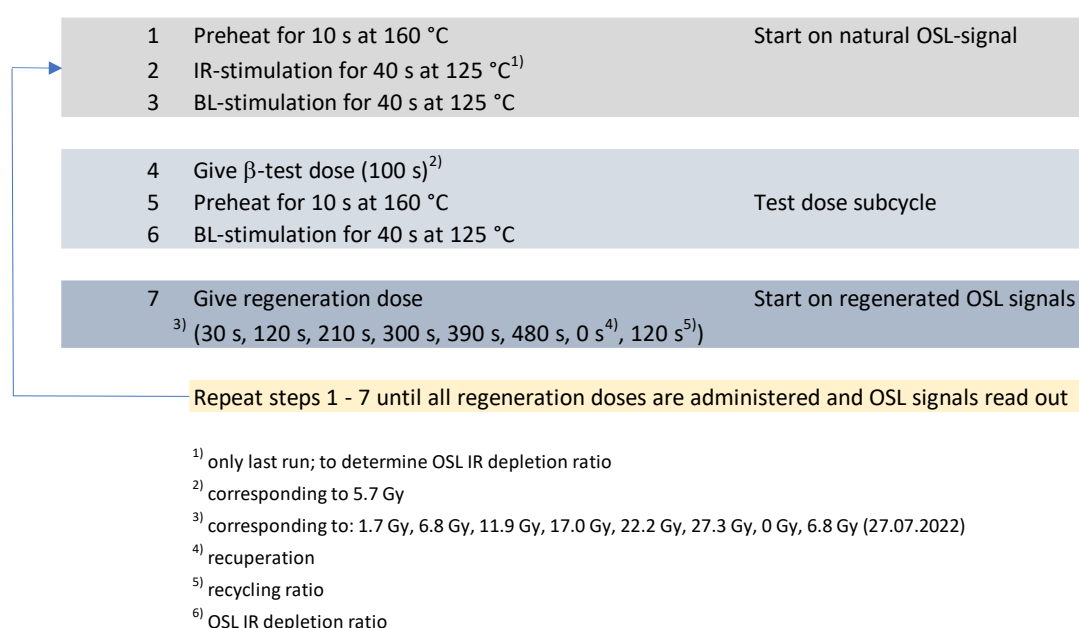


Figure S19. Schematic representation of the BLSL₁₂₅ SAR protocol adapted to quartz coarse grain separates (125–212 μm) from the sand infill of the trenches in this study.

SAR measurements

Results of the D_e determination for samples HDS-1818 to HDS-1823 are given in Figs. S20–S27 and Tables S5–S12. Twenty-four aliquots were measured of each of the samples HDS-1818 to HDS-1821, 48 aliquots of sample HDS-1823 and 144 aliquots of sample HDS-1822, which appeared to be the best bleached sample, as deduced from the D_e distribution of the first 48 measured aliquots. Altogether 288 aliquots were measured from the six samples, which seem to represent one and the same depositional event (within a likely time interval of a few days to a few weeks).

D_e determination occurred for the D_e integral 0–0.1 s and 0–0.4 s, respectively, to investigate if the samples show insufficient bleaching, e.g., by systematically larger D_e values for the longer D_e integral. Instead, the comparison of the two different D_e integrals, with the integral 30.1–40 s used for late light subtraction, revealed systematically smaller D_e s for the longer D_e interval. This phenomenon may point to an instable medium and/or slow component of the quartz luminescence signal (Li and Li, 2006) and/or charge retrapping from a shallow trap, which had not been emptied during preheating.

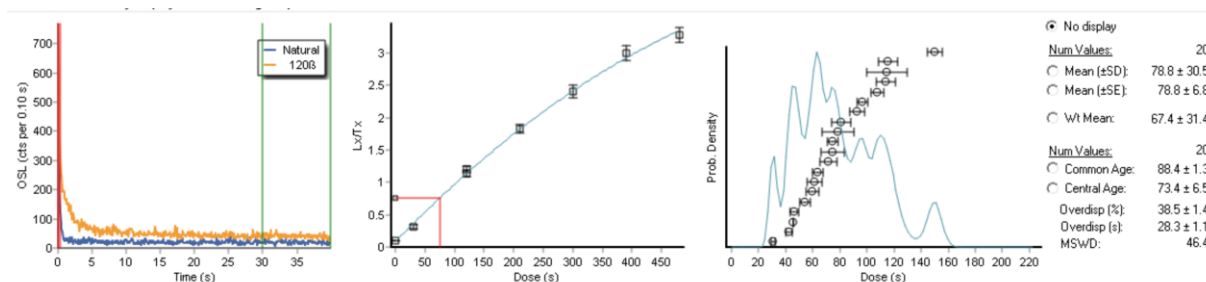


Figure S20: De determination on sample HDS-1818. Example of shine down curve, dose response curve with an exponential plus linear fit and weighted histogram of all analysable aliquots (N = 20 for De interval 0–0.4 s).

Table S5. Recovered De values for the different integrals (sample HDS-1818). De values for integral 0–0.4 s are systematically smaller than those for the De integral 0–0.1 s. Table cells marked in pink denote aliquots eliminated due to an OSL IR depletion ratio $\geq 10\%$ pointing to feldspar contamination.

turntable position [#]	aliquot [#]	determined dose [s irradiation time] [0 - 0.1 s]	determined dose [s irradiation time] [0 - 0.4 s]	Diff long vs. short De interval [s irradiation time] [0 - 0.4 s] - [0 - 0.1 s]
1	1	n.a.	n.a.	
2	2	85.74	6.62	75.05
3	3		n.a.	4.41
4	4	83.75	14.24	78.55
5	5	67.99	9.98	11.44
6	6	121.78	11.24	42.10
7	7	42.83	7.58	5.18
8	8	n.a.		7.44
9	9	73.09	7.52	45.41
10	10	105.57	5.95	4.48
11	11	71.73	11.73	74.98
12	12	89.95	9.79	8.41
13	13	125.86	13.20	5.09
14	14	57.20	6.87	59.59
15	15	106.32	5.35	5.09
16	16	41.13	2.83	59.59
17	17	n.a.		96.70
18	18	89.39	9.57	4.26
19	19	n.a.		61.55
20	20	124.71	8.78	5.53
21	21	n.a.		5.53
22	22	146.04	6.08	6.73
23	23	59.99	9.07	6.00
24	24	84.40	4.92	6.00

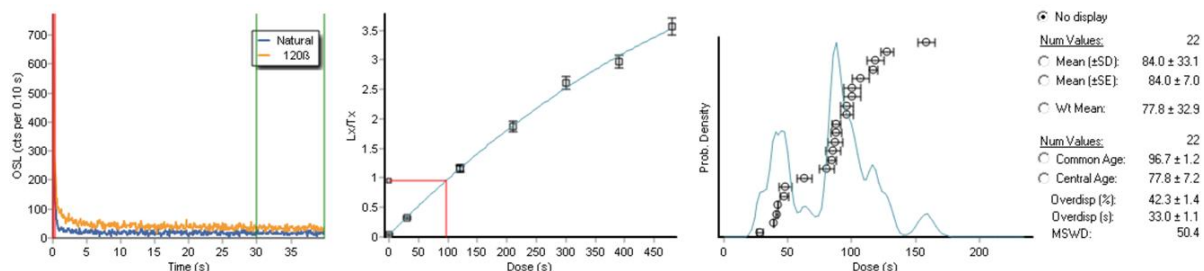


Figure S21. De determination on sample HDS-1819. Example of shine down curve, dose response curve with an exponential plus linear fit and weighted histogram of all analysable aliquots (N = 22 for De interval 0–0.4 s).

Table S6. Recovered De values for the different integrals (sample HDS-1819). Des for the De integral 0–0.4 s are systematically smaller than those for the De integral 0–0.1 s. The table cell marked in pink denote aliquots eliminated due to an OSL IR depletion ratio ≥ 10 % pointing to feldspar contamination.

turntable position	aliquot	determined dose		determined dose		Diff long vs. short De interval
[#]	[#]	[s irradiation time]	[s irradiation time]	[s irradiation time]	[s irradiation time]	[s irradiation time]
		[0 - 0.1 s]	[0 - 0.4 s]	[0 - 0.4 s]	[0 - 0.4 s]	[0 - 0.1 s]
25	1	106.10	7.33	96.75	5.22	-9.35
26	2	211.63	10.56	158.41	6.53	-53.22
27	3	62.03	11.50	42.31	7.08	-19.72
28	4	44.86	5.20	28.63	3.90	-16.23
29	5	65.29	4.69	47.16	3.84	-18.13
30	6	101.88	5.20	87.71	4.05	-14.17
31	7	n.a.		96.39	5.39	
32	8	118.13	4.29	116.88	3.60	-1.25
33	9	n.a.		n.a.		
34	10	116.02	8.93	100.38	5.97	-15.64
35	11					
36	12	108.61	8.76	106.98	6.32	-1.63
37	13	146.85	7.09	127.93	4.83	-18.92
38	14	60.26	7.60	48.33	4.34	-11.93
39	15	101.82	5.47	84.87	3.61	-16.95
40	16	52.06	5.44	38.82	2.94	-13.24
41	17	67.91	13.13	41.19	5.91	-26.72
42	18	99.17	8.12	85.75	5.92	-13.42
43	19	124.50	11.48	100.82	6.73	-23.68
44	20	88.30	11.98	80.46	9.27	-7.84
45	21	80.91	7.86	63.10	5.49	-17.81
46	22	94.40	4.94	87.79	3.50	-6.61
47	23	119.20	9.44	118.84	7.33	-0.36
48	24	115.55	7.32	87.57	5.34	-27.98

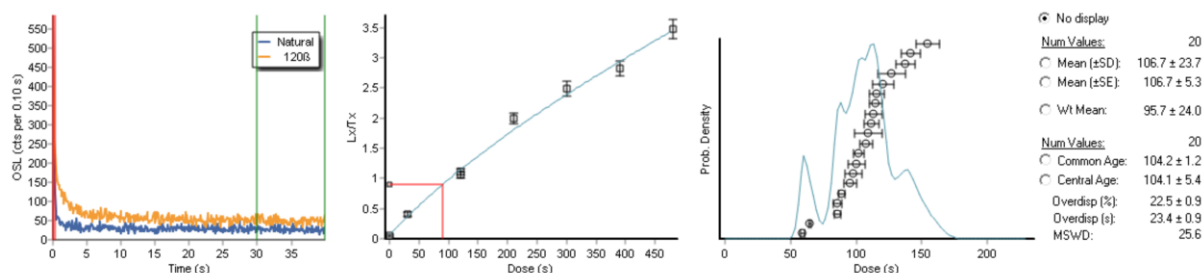


Figure S22. De determination on sample HDS-1820. Example of shine down curve, dose response curve with an exponential plus linear fit and weighted histogram of all analysable aliquots (N = 20 for De interval 0–0.4 s).

Table S7. Recovered De values for the different integrals (sample HDS-1820). Des for the De integral 0–0.4 s are systematically smaller than those for the De integral 0–0.1 s. Table cells marked in pink denote aliquots eliminated due to an OSL IR depletion ratio $\geq 10\%$ pointing to feldspar contamination.

turntable position	aliquot	determined dose	determined dose	Diff long vs. short De interval	
[#]	[#]	[s irradiation time] [0 - 0.1 s]	[s irradiation time] [0 - 0.4 s]	[s irradiation time] [0 - 0.4 s] - [0 - 0.1 s]	
1	1	99.72	11.38	89.28	6.75
2	2	111.77	6.03	107.84	4.59
3	3	134.02	8.71	137.58	6.58
4	4	120.13	14.17	109.07	10.73
5	5	120.26	9.84	113.42	6.67
6	6	88.94	11.80	85.65	7.10
7	7				
8	8	65.11	5.83	65.01	4.25
9	9	136.07	10.01	141.31	7.55
10	10	89.32	3.13	86.13	3.14
11	11				
12	12	112.06	6.97	111.48	6.01
13	13	105.74	7.39	95.71	4.81
14	14	121.00	6.40	114.79	4.74
15	15	104.39	4.24	102.10	3.37
16	16				
17	17	104.09	12.78	126.79	10.69
18	18	154.89	11.31	154.31	8.66
19	19	107.06	10.42	97.59	6.77
20	20	74.25	5.18	59.27	3.10
21	21				
22	22	133.30	10.15	116.10	5.94
23	23	137.32	13.40	120.99	7.90
24	24	118.13	13.24	99.96	8.43

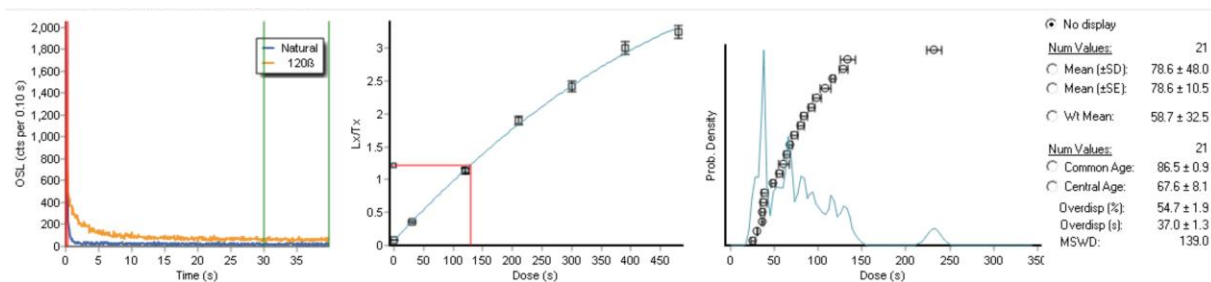


Figure S23. De determination on sample HDS-1821. Example of shine down curve, dose response curve with an exponential plus linear fit and weighted histogram of all analysable aliquots (N = 21 for De interval 0–0.4 s).

Table S8. Recovered De values for the different integrals (sample HDS-1821). Des for the De interval 0–0.4 s are systematically smaller than those for the De interval 0–0.1 s. Table cells marked in pink denote aliquots eliminated due to an OSL IR depletion ratio $\geq 10\%$ pointing to feldspar contamination.

turntable position	aliquot	determined dose	determined dose	Diff long vs. short De interval
[#]	[#]	[s irradiation time]	[s irradiation time]	[s irradiation time]
		[0 - 0.1 s]	[0 - 0.4 s]	[0 - 0.4 s] - [0 - 0.1 s]
25	1	144.41	12.25	134.23
26	2			8.19
27	3	149.42	7.69	128.70
28	4	85.13	5.90	79.98
29	5	98.94	4.36	91.94
30	6	87.49	5.17	83.98
31	7	76.67	4.70	64.94
32	8	38.23	2.49	37.07
33	9	53.21	6.10	38.71
34	10	80.20	6.52	73.54
35	11	111.23	7.96	98.85
36	12	52.67	4.78	37.33
37	13			
38	14	38.58	2.83	37.07
39	15	49.05	4.77	49.21
40	16	84.93	4.11	67.64
41	17	274.59	11.44	231.84
42	18	36.82	3.73	25.27
43	19			
44	20	74.69	7.10	55.78
45	21	118.36	4.01	116.30
46	22	112.84	7.21	108.49
47	23	61.93	8.38	60.32
48	24	42.45	5.24	30.11

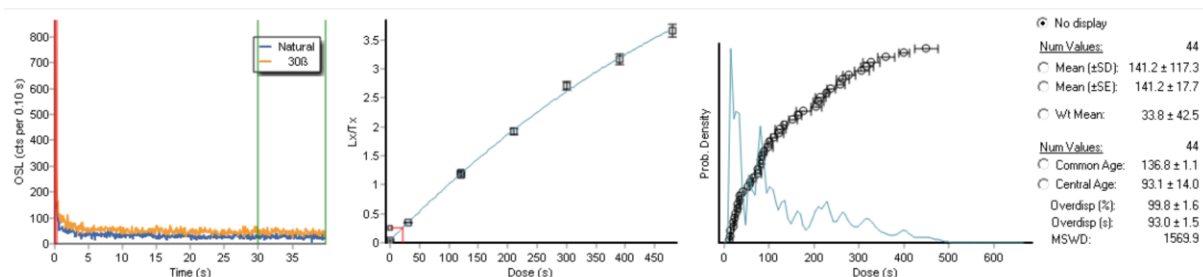


Figure S24. De determination on sample HDS-1822 (aliquots 1–48). Example of shine down curve, dose response curve with an exponential plus linear fit and weighted histogram of all analysable aliquots (N = 44 for De interval 0–0.4 s).

Table S9. Recovered De values for the different integrals (sample HDS-1822, aliquots 1–48). Des for the De interval 0–0.4 s are systematically smaller than those for the De interval 0–0.1 s. Table cells marked in pink denote aliquots eliminated due to an OSL IR depletion ratio $\geq 10\%$ pointing to feldspar contamination. For two aliquots with the smallest Des no trend of decreasing De with increasing length of the De interval was observed.

turntable position [#]	aliquot [#]	determined dose [s irradiation time] [0 - 0.1 s]		determined dose [s irradiation time] [0 - 0.4 s]		Diff long vs. short De interval [s irradiation time] [0 - 0.4 s] - [0 - 0.1 s]
	1	1	186.94	8.51	236.81	8.82
	2	2	113.13	10.06	110.18	6.89
	3	3	266.14	7.82	228.06	6.29
	4	4	386.21	22.47	318.70	13.98
	5	5	164.51	13.44	152.14	9.25
	6	6	56.80	3.11	55.04	2.72
	7	7	218.53	24.37	176.82	14.71
	8	8	21.37	1.77	21.34	1.60
	9	9	348.77	23.59	306.79	16.33
	10	10	25.84	2.70	25.46	1.75
	11	11	15.11	1.39	15.11	1.09
	12	12	43.36	3.17	31.66	2.26
	13	13	n.a.		400.40	12.97
	14	14	22.28	2.41	21.70	2.03
	15	15	554.57	39.02	448.82	25.90
	16	16	106.64	6.89	90.06	4.53
	17	17	210.05	12.14	164.97	7.19
	18	18	9.88	1.70	11.00	1.58
	19	19	314.57	18.97	264.69	12.24
	20	20	193.38	10.61	133.09	5.56
	21	21	33.45	3.60	34.30	3.31
	22	22			n.a.	
	23	23			n.a.	
	24	24	97.07	10.55	83.81	5.37
	25	25	262.04	18.67	203.67	10.56
	26	26	48.35	8.02	35.23	5.62
	27	27	376.99	34.29	326.75	18.83
	28	28	100.70	7.94	81.76	6.25
	29	29	37.66	5.13	29.80	4.07
	30	30	83.27	6.35	75.25	4.57
	31	31			n.a.	
	32	32	104.32	5.16	82.20	3.33
	33	33	14.77	1.54	13.89	1.00
	34	34	207.41	25.72	122.60	11.21
	35	35	316.87	15.60	259.05	10.21
	36	36	25.97	1.69	24.64	1.44
	37	37	254.70	17.59	214.14	11.10
	38	38	314.88	20.39	277.04	13.92
	39	39	100.40	8.77	66.51	5.12
	40	40	161.02	8.79	102.24	4.84
	41	41	392.60	27.24	360.46	19.09
	42	42	249.67	18.54	208.57	11.94
	43	43	42.99	2.73	43.36	2.20
	44	44	55.72	4.19	57.80	3.09
	45	45	0.45		n.a.	
	46	46	112.49	11.60	74.49	6.24
	47	47	161.58	18.83	124.92	11.65
	48	48	119.58	18.93	99.21	9.27

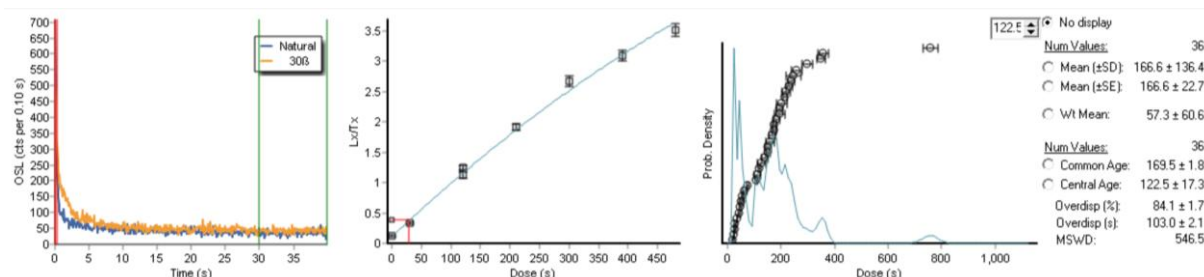


Figure S25. De determination on sample HDS-1822 (aliquots 49–96). Example of shine down curve, dose response curve with an exponential plus linear fit and weighted histogram of all analysable aliquots (N = 36 for De interval 0–0.4 s).

Table S10. Recovered De values for the different integrals (sample HDS-1822, aliquots 49–96). Des for the De interval 0–0.4 s are systematically smaller than those for the De interval 0–0.1 s. Table cells marked in pink denote aliquots eliminated due to an OSL IR depletion ratio $\geq 10\%$ pointing to feldspar contamination. For two aliquots with the smallest Des no trend of decreasing De with increasing length of the De interval was observed.

turntable position [#]	aliquot [#]	determined dose [s irradiation time] [0 - 0.1 s]		determined dose [s irradiation time] [0 - 0.4 s]		Diff long vs. short De interval [s irradiation time] [0 - 0.4 s] - [0 - 0.1 s]
1	1	727.15	30.16	757.72	29.11	30.57
2	2	39.91	7.74			-39.91
3	3					
4	4	398.07	28.36	349.56	17.67	-48.51
5	5					
6	6					
7	7	40.61	3.92	29.62	3.73	-10.99
8	8	39.24	5.26	46.67	4.22	7.43
9	9	227.66	21.51	218.94	14.99	-8.72
10	10					
11	11	140.95	5.48	119.40	4.78	-21.55
12	12	37.56	2.00	36.96	1.56	-0.60
13	13	298.34	27.49	230.78	14.17	-67.56
14	14	185.24	16.00	166.58	10.97	-18.66
15	15	33.15	4.92	20.68	3.05	-12.47
16	16	298.84	24.40	299.60	19.94	0.76
17	17	256.52	11.09	213.10	7.85	-43.42
18	18	174.56	16.56	149.59	10.05	-24.97
19	19	n.a.		61.91	9.20	
20	20					
21	21	514.33	60.41			-514.33
22	22	223.19	14.04	193.39	10.73	-29.80
23	23	34.01	5.52	27.99	3.45	-6.02
24	24	199.62	16.29	176.06	10.05	-23.56
25	25			109.33	12.00	109.33
26	26	47.65	6.51	45.39	5.03	-2.26
27	27					
28	28	348.07	36.37	256.46	20.50	-91.61
29	29	232.28	29.22	201.53	20.26	-30.75
30	30					
31	31	n.a.		75.78	16.94	
32	32	130.08	9.26	105.89	4.71	-24.19
33	33	412.96	23.10	357.82	18.17	-55.14
34	34					
35	35	387.72		245.68	26.75	-142.04
36	36	48.99	14.85	50.31	7.85	1.32
37	37	297.97	18.56	239.08	11.73	-58.89
38	38	209.65	21.91	152.94	11.95	-56.71
39	39	199.51	15.98	182.42	11.19	-17.09
40	40	180.80	10.90	176.03	8.37	-4.77
41	41	n.a.		126.22	15.82	
42	42	n.a.		193.08	20.37	
43	43	n.a.		56.92	12.67	
44	44	n.a.				
45	45	186.77	23.15	139.86	12.03	-46.91
46	46	23.74	2.90	22.88	2.28	-0.86
47	47	n.a.		159.94	12.67	
48	48	n.a.		n.a.		

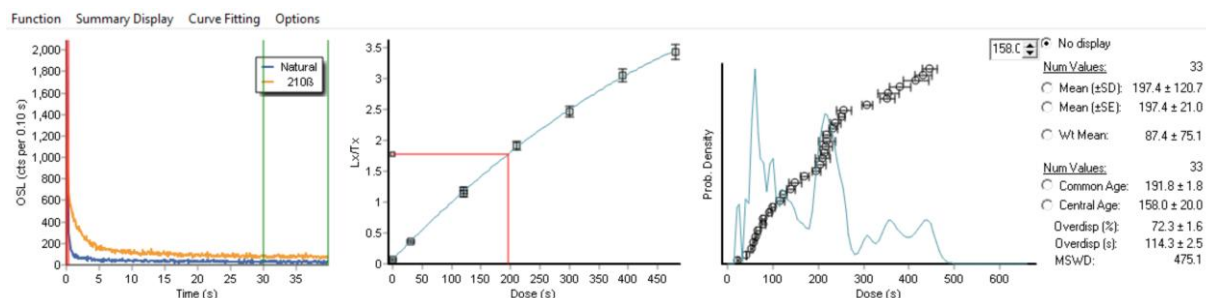


Figure S26. De determination on sample HDS-1822 (aliquots 97–144). Example of shine down curve, dose response curve with an exponential plus linear fit and weighted histogram of all analysable aliquots (N = 33 for De interval 0–0.4 s).

Table S11. Des for the De integral 0–0.4 s are systematically smaller than those for the De integral 0–0.1 s. Table cells marked in pink denote aliquots eliminated due to an OSL IR depletion ratio $\geq 10\%$ pointing to feldspar contamination. Cells marked in green denote aliquots which do not show a decreasing De value with increasing length of the De interval (here 0.4 s vs 0.1 s).

turntable position [#]	aliquot [#]	determined dose [s irradiation time] [0 - 0.1 s]		determined dose [s irradiation time] [0 - 0.4 s]		Diff long vs. short De interval [s irradiation time] [0 - 0.4 s] - [0 - 0.1 s]
	1	248.59	15.09	196.28	8.06	-52.31
	2	103.83	8.94	79.67	5.38	-24.16
	3					
	4	254.92	14.03	214.43	9.39	-40.49
	5	n.a.		140.02	9.04	
	6					
	7	474.85		432.82	19.43	-42.03
	8	277.05	12.41	233.60	8.13	-43.45
	9	139.72	18.47	115.78	9.60	-23.94
	10	n.a.		218.34	17.06	
	11	106.15	15.22	78.57	9.17	-27.58
	12					
	13	272.00	11.55	252.62	8.89	-19.38
	14	72.48	7.42	67.31	4.39	-5.17
	15	456.03	39.06	415.68	28.82	-40.35
	16					
	17	455.75	26.63	352.91	14.95	-102.84
	18	32.74	8.67	23.43	2.94	-9.31
	19			62.56	7.87	62.56
	20	441.03		380.96	23.64	-60.07
	21	262.18	22.57	216.65	14.32	-45.53
	22	118.32	7.20	101.25	5.01	-17.07
	23	n.a.				
	24					
	25	405.21	43.43	355.70	24.60	-49.51
	26	314.10	26.52	257.03	15.27	-57.07
	27	n.a.				
	28	262.85	16.79	239.02	12.10	-23.83
	29	166.71	12.38	122.92	7.94	-43.79
	30	36.31	4.42	43.08	3.28	6.77
	31	108.59	7.22	94.05	4.84	-14.54
	32					
	33	54.13	3.04	59.05	2.56	4.92
	34	253.57	29.00	210.30	17.81	-43.27
	35	210.57	16.99	205.76	12.57	-4.81
	36	374.52	20.10	306.95	12.37	-67.57
	37	476.84		444.96	15.44	-31.88
	38	188.51	17.21	169.20	10.98	-19.31
	39					
	40	211.83	27.01	148.68	13.65	-63.15
	41	48.53	3.17	54.56	2.67	6.03
	42	275.88	19.56	219.17	10.78	-56.71
	43	Messung abgebrochen	Messung abgebrochen			
	44					
	45					
	46					
	47					
	48					

HDS-1823 – 48 measured aliquots

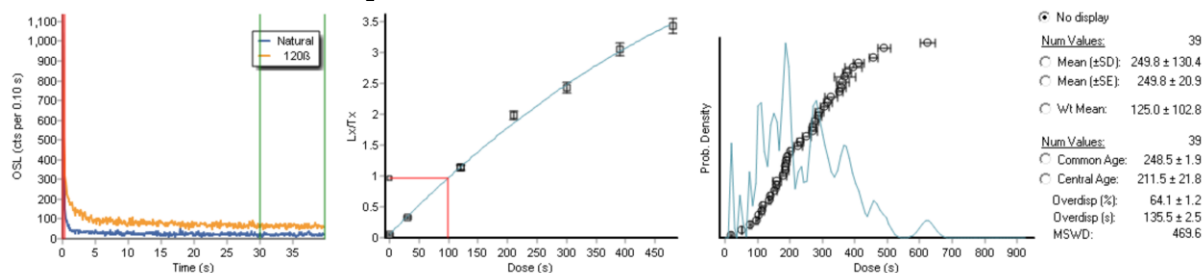


Fig. S27. De determination on sample HDS-1823. Example of shine down curve, dose response curve with an exponential plus linear fit and weighted histogram of all analysable aliquots (N = 39 for De interval 0–0.4 s).

Table S12. Des for the De integral 0–0.4 s are systematically smaller than those for the De integral 0–0.1 s. Table cells marked in pink denote aliquots eliminated due to an OSL IR depletion ratio ≥ 10 % pointing to feldspar contamination.

turntable position [#]	aliquot [#]	determined dose [s irradiation time] [0 - 0.1 s]		determined dose [s irradiation time] [0 - 0.4 s]		Diff long vs. short De interval [s irradiation time] [0 - 0.4 s] - [0 - 0.1 s]
1	1	453.02	12.34	458.52	12.66	5.50
2	2	367.94	26.52	224.79	10.84	-143.15
3	3					
4	4					
5	5	337.60	24.18	326.71	18.94	-10.89
6	6	143.34	8.54	140.23	6.82	-3.11
7	7	329.54	15.49	270.99	10.08	-58.55
8	8	150.45	16.64	136.45	10.01	-14.00
9	9	346.73	24.10	317.72	14.25	-29.01
10	10	n.a.		161.29	11.62	
11	11	287.73	45.91	353.64	47.68	65.91
12	12	128.44	8.07	78.20	4.03	-50.24
13	13	299.78	20.34	232.48	10.87	-67.30
14	14	424.39	40.21	394.65	25.27	-29.74
15	15	317.21	16.95	270.58	11.30	-46.63
16	16	430.38	31.03	362.16	18.69	-68.22
17	17					
18	18	215.66	14.11	190.08	9.31	-25.58
19	19	331.14	23.34	290.48	13.73	-40.66
20	20	192.67	15.37	187.42	10.04	-5.25
21	21	247.55	14.85	192.48	8.13	-55.07
22	22	168.96	17.14	159.59	12.18	-9.37
23	23	n.a.		118.17	7.55	
24	24	375.45	48.47	n.a.		
25	25	642.61	27.26	623.61	21.80	-19.00
26	26	340.32	18.27	278.13	11.75	-62.19
27	27					
28	28	n.a.		371.20	31.15	
29	29					
30	30	n.a.		479.05		
31	31	373.69	19.46	306.51	11.93	-67.18
32	32					
33	33	281.93	20.84	252.04	13.83	-29.89
34	34	427.76	20.06	411.53	16.49	-16.23
35	35	396.17	17.06	377.71	14.34	-18.46
36	36					
37	37	118.21	6.96	98.94	4.66	-19.27
38	38	165.22	11.94	112.86	6.22	-52.36
39	39	140.53	10.95	105.46	6.90	-35.07
40	40	403.85	16.89	360.11	14.64	-43.74
41	41	58.03	3.99	50.75	2.48	-7.28
42	42	210.69	12.03	154.46	6.51	-56.23
43	43	222.60	18.44	187.85	11.24	-34.75
44	44	33.38	4.26	20.88	3.18	-12.50
45	45	246.35	15.39	181.34	7.85	-65.01
46	46	360.12	16.74	288.65	10.88	-71.47
47	47	245.00	10.85	202.50	6.97	-42.50
48	48	523.20	27.29	489.13	18.39	-34.07

Further tests

For the SAR measurements of the natural dose the six OSL samples all show a tendency of smaller D_{es} for the longer D_e intervals 0–0.4 s as compared to the shorter D_e interval 0–0.1 s. This is in contrast to the dose recovery test, for which the different D_e intervals provided very similar D_e values within error margins (Table S4). Therefore, we performed linear modulated OSL (LM-OSL) tests and a crosscheck on another luminescence reader.

LM-OSL test

We performed LM-OSL measurements on five aliquots of sample HDS-1822, measuring both first the natural OSL signal and subsequently a regenerated signal of each aliquot to investigate whether the samples may be dominated by an instable medium or slow component (Figs. S28–S36). As for the D_e measurements the LM-OSL measurement was performed with the blue LEDs (BLSL; 470 nm) increasing the LED power over 4000 s up to 90 %. The analysis was performed with the `fit_LMCurve` function of the R package *Luminescence* (Kreutzer et al., 2012; Kreutzer et al., 2024) determining the relative contribution of four assumed components to the sum curve of the BLSL signal curve. The cross sections of the first component were in all cases $\leq 10^{-17} \text{ cm}^2$ pointing to a dominant fast component.

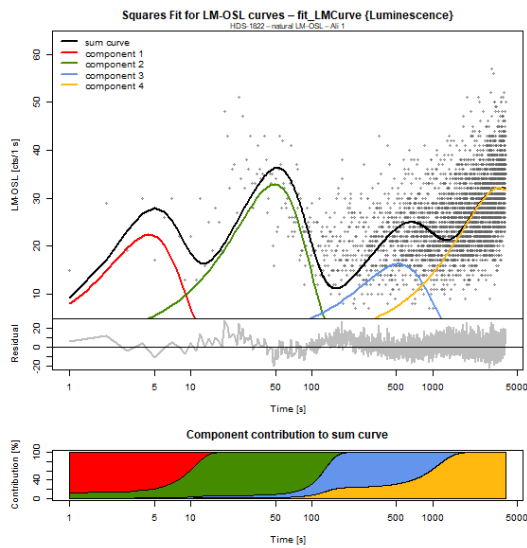


Figure S28: HDS-1822 – LM-OSL test, first aliquot, natural LM-OSL signal (DA15, 90 % LED power, 470 nm, four components).

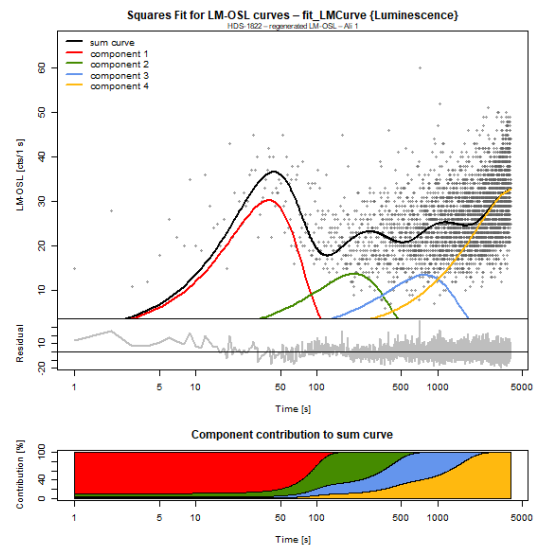


Figure S29. HDS-1822 – LM-OSL test, first aliquot, regenerated LM-OSL signal (DA15, 90 % LED power, 470 nm, four components).

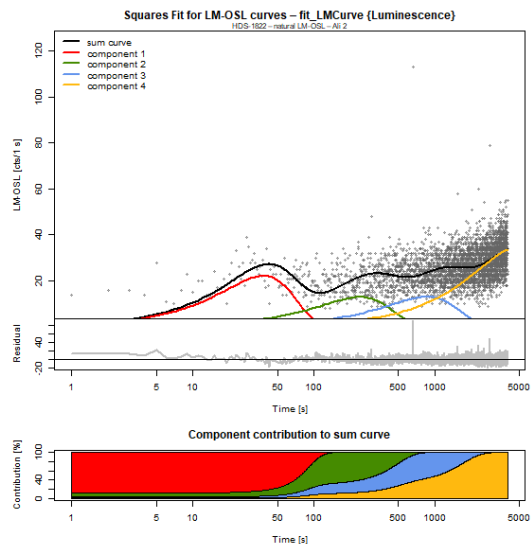


Figure S30. HDS-1822 – LM-OSL test, second aliquot, natural LM-OSL signal (DA15, 90 % LED power, 470 nm, four components).

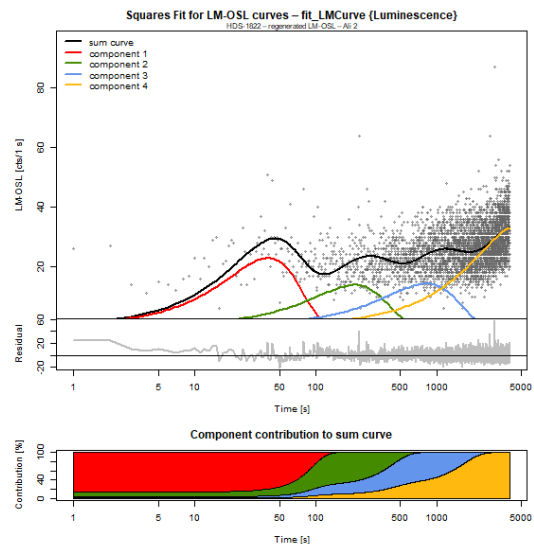


Figure S30. HDS-1822 – LM-OSL test, second aliquot, regenerated LM-OSL signal (DA15, 90 % LED power, 470 nm, four components).

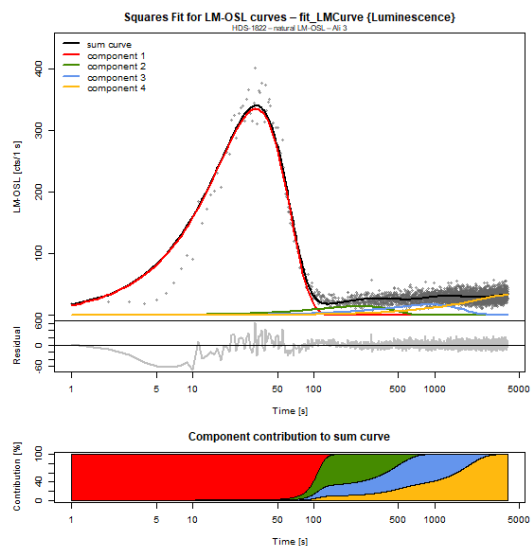


Figure S31. HDS-1822 – LM-OSL test, third aliquot, natural LM-OSL signal (DA15, 90 % LED power, 470 nm, four components).

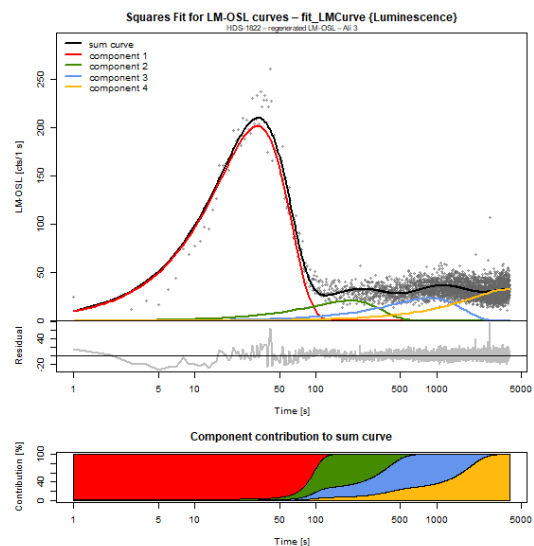


Figure S32. HDS-1822 – LM-OSL test, third aliquot, regenerated LM-OSL signal (DA15, 90 % LED power, 470 nm, four components).

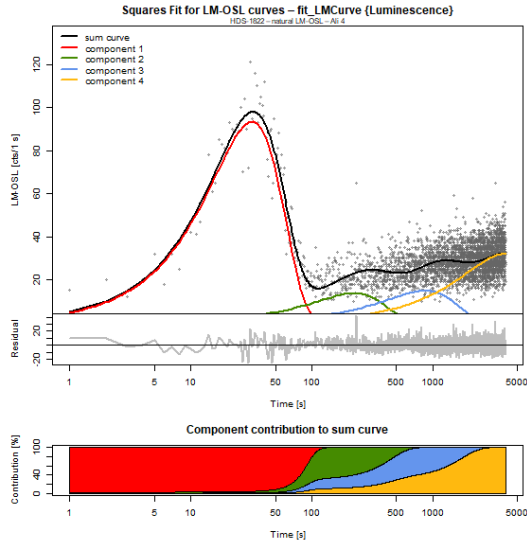


Figure S33. HDS-1822 – LM-OSL test, fourth aliquot, natural LM-OSL signal (DA15, 90 % LED power, 470 nm, four components).

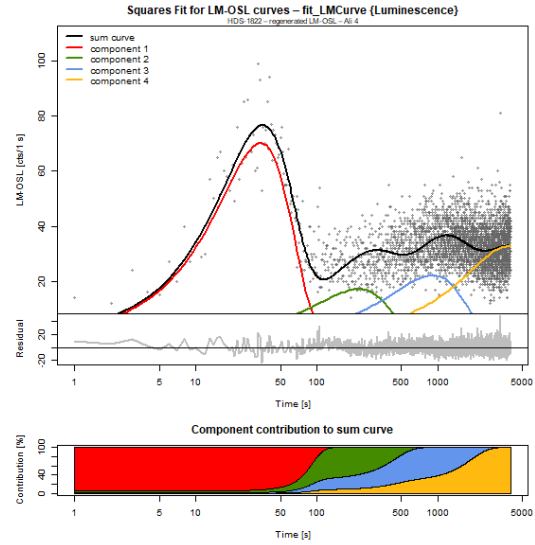


Figure S34. HDS-1822 – LM-OSL test, fourth aliquot, regenerated LM-OSL signal (DA15, 90 % LED power, 470 nm, four components).

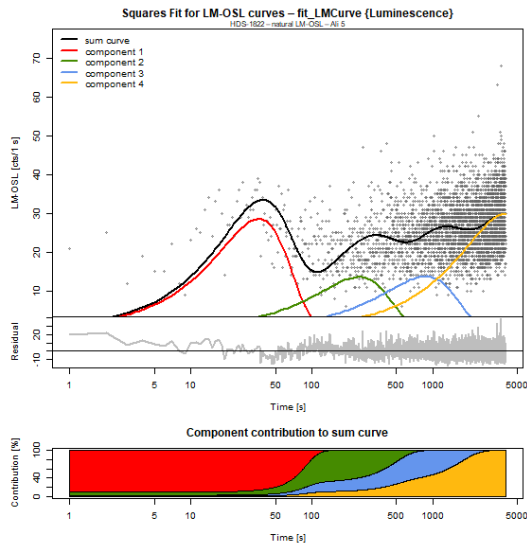


Figure S35. HDS-1822 – LM-OSL test, fifth aliquot, natural LM-OSL signal (DA15, 90 % LED power, 470 nm, four components).

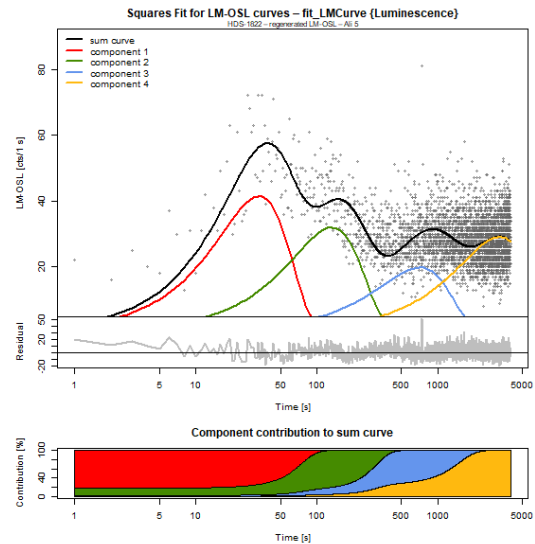


Figure S36. HDS-1822 – LM-OSL test, fifth aliquot, regenerated LM-OSL signal (DA15, 90 % LED power, 470 nm, four components).

Crosscheck on a different luminescence reader

In addition, we measured 24 aliquots of sample HDS-1822 on a different luminescence reader (DA20; No. 245) (DTU Physics, 2021) to check whether the phenomenon of De value decline with increasing De interval length is due to a malfunction of the luminescence reader. This assumption could be excluded, as the aliquots measured on DA20 (No. 245) showed the same peculiarity.

Dose rate determination

For radionuclide determination the μ Dose system (Tudyka et al., 2018; Kolb et al., 2022) was used, performing two measurements, over one day each, on each sample. Despite slight differences in the

determined radionuclide contents of uranium and thorium the effective total dose rates conform within error ranges (Table S13). The cosmic dose rate was calculated applying the function `calc_CosmicDoseRate` (Burow, 2024) of the R package `Luminescence` (Kreutzer et al., 2012). For determining the effective dose rates the dose-rate conversion factors of Guerin et al. (2011) and a water content of 1.05 ± 0.05 (sample's wet weight/sample's dry weight) were considered.

Table S13. Essential data for age calculation. Ages in the upper part are based on the central age model (CAM; Galbraith et al., 1999). Ages in the lower part are based on the minimum age model (MAM; Galbraith et al., 1999) using sigma_b = 0.2 and the 1 sigma level (0.68) as parameters. Blue shaded samples are from Pit 1, green shaded samples are from Pit 2, orange shaded rows indicate all six samples from both pits.

Lab.-No. [HDS-No.]	De [Gy]	Aliquots [N]	OD [%]	Dose rate, cosmic [Gy/ka]			U [μg/g]	Th [μg/g]	K [μg/g]	Water content (error as modelled) Δ [wet weight/dry weight]		eff. β dose rate [Gy/ka]	eff. γ dose rate [Gy/ka]	effective dose rate [Gy/ka]	age [ka]	mean eff. dose rate [Gy/ka]						
1 HDS-1818 - CAM	4.17	± 0.37	20	38.43	± 6.42	0.182	± 0.018	0.7895	± 0.188	3.1662	± 0.646	1.3636	± 0.057	1.05	± 0.05	1.151	0.548	1.881	± 0.101	2.22	± 0.23	1.8353 ± 0.0456
2 HDS-1818 - CAM	4.17	± 0.37	20	38.43	± 6.42	0.182	± 0.018	0.9780	± 0.202	1.5648	± 0.681	1.3354	± 0.057	1.05	± 0.05	1.119	0.489	1.790	± 0.100	2.33	± 0.24	
3 HDS-1819 - CAM	4.42	± 0.41	22	42.22	± 6.63	0.189	± 0.019	0.8836	± 0.209	2.6683	± 0.691	1.2606	± 0.062	1.05	± 0.05	1.077	0.511	1.777	± 0.101	2.49	± 0.27	
4 HDS-1819 - CAM	4.42	± 0.41	22	42.22	± 6.63	0.189	± 0.019	0.5255	± 0.213	4.5025	± 0.735	1.3331	± 0.064	1.05	± 0.05	1.126	0.574	1.888	± 0.106	2.34	± 0.25	1.8128 ± 0.0532
5 HDS-1819 - CAM	4.42	± 0.41	22	42.22	± 6.63	0.189	± 0.019	0.9532	± 0.193	2.5911	± 0.637	1.2463	± 0.062	1.05	± 0.05	1.073	0.512	1.774	± 0.099	2.49	± 0.27	
6 HDS-1820 - CAM	5.91	± 0.31	20	22.28	± 3.87	0.197	± 0.020	0.4891	± 0.209	4.1168	± 0.705	1.4681	± 0.059	1.05	± 0.05	1.211	0.584	1.992	± 0.107	2.97	± 0.22	
7 HDS-1820 - CAM	5.91	± 0.31	20	22.28	± 3.87	0.197	± 0.020	0.5808	± 0.214	3.9092	± 0.723	1.4201	± 0.060	1.05	± 0.05	1.183	0.573	1.953	± 0.106	3.03	± 0.23	1.9533 ± 0.0318
8 HDS-1820 - CAM	5.91	± 0.31	20	22.28	± 3.87	0.197	± 0.020	0.4314	± 0.202	4.2312	± 0.688	1.3928	± 0.059	1.05	± 0.05	1.152	0.566	1.914	± 0.103	3.09	± 0.23	
9 HDS-1821 - CAM	3.84	± 0.46	21	54.67	± 8.58	0.186	± 0.019	0.9839	± 0.205	2.0734	± 0.691	1.3363	± 0.057	1.05	± 0.05	1.131	0.513	1.830	± 0.101	2.10	± 0.28	
10 HDS-1821 - CAM	3.84	± 0.46	21	54.67	± 8.58	0.186	± 0.019	0.8241	± 0.232	2.2974	± 0.790	1.3608	± 0.058	1.05	± 0.05	1.135	0.512	1.832	± 0.105	2.10	± 0.28	1.8635 ± 0.0326
11 HDS-1821 - CAM	3.84	± 0.46	21	54.67	± 8.58	0.186	± 0.019	0.3115	± 0.461	4.3166	± 1.632	1.4113	± 0.084	1.05	± 0.05	1.153	0.561	1.900	± 0.155	2.02	± 0.29	
12 HDS-1821 - CAM	3.84	± 0.46	21	54.67	± 8.58	0.186	± 0.019	0.7224	± 0.203	2.1328	± 0.692	1.4585	± 0.058	1.05	± 0.05	1.190	0.517	1.892	± 0.104	2.03	± 0.27	
13 HDS-1822 - CAM	6.73	± 0.57	113	90.13	± 6.05	0.190	± 0.019	0.8201	± 0.211	3.1957	± 0.704	1.2866	± 0.062	1.05	± 0.05	1.099	0.535	1.824	± 0.103	3.69	± 0.38	1.8728 ± 0.0490
14 HDS-1822 - CAM	6.73	± 0.57	113	90.13	± 6.05	0.190	± 0.019	0.9909	± 0.173	1.8727	± 0.561	1.4402	± 0.063	1.05	± 0.05	1.203	0.529	1.922	± 0.103	3.50	± 0.35	
15 HDS-1823 - CAM	12.25	± 1.26	40	64.56	± 7.29	0.194	± 0.019	0.9971	± 0.215	2.6063	± 0.702	1.2555	± 0.058	1.05	± 0.05	1.086	0.519	1.799	± 0.101	6.81	± 0.80	
16 HDS-1823 - CAM	12.25	± 1.26	40	64.56	± 7.29	0.194	± 0.019	0.7542	± 0.210	3.2552	± 0.697	1.4606	± 0.060	1.05	± 0.05	1.219	0.571	1.985	± 0.107	6.17	± 0.72	1.8919 ± 0.0928
17 All - CAM	6.47	± 0.34	236	80.35	± 3.74	0.190	± 0.019	0.7522	± 0.215	3.0313	± 0.921	1.3644	± 0.073	1.05	± 0.05	1.144	0.538	1.872	± 0.114	3.46	± 0.28	
19 HDS-1818 - MAM	2.67	± 0.21	20	38.43	± 6.42	0.182	± 0.018	0.7895	± 0.188	3.1662	± 0.646	1.3636	± 0.057	1.05	± 0.05	1.151	0.548	1.881	± 0.101	1.42	± 0.14	1.8353 ± 0.0456
20 HDS-1818 - MAM	2.67	± 0.21	20	38.43	± 6.42	0.182	± 0.018	0.9780	± 0.202	1.5648	± 0.681	1.3354	± 0.057	1.05	± 0.05	1.119	0.489	1.790	± 0.100	1.49	± 0.14	
21 HDS-1819 - MAM	2.52	± 0.20	22	42.22	± 6.63	0.189	± 0.019	0.8836	± 0.209	2.6683	± 0.691	1.2606	± 0.062	1.05	± 0.05	1.077	0.511	1.777	± 0.101	1.42	± 0.14	
22 HDS-1819 - MAM	2.52	± 0.20	22	42.22	± 6.63	0.189	± 0.019	0.5255	± 0.213	4.5025	± 0.735	1.3331	± 0.064	1.05	± 0.05	1.126	0.574	1.888	± 0.106	1.33	± 0.13	1.8128 ± 0.0532
23 HDS-1819 - MAM	2.52	± 0.20	22	42.22	± 6.63	0.189	± 0.019	0.9532	± 0.193	2.5911	± 0.637	1.2463	± 0.062	1.05	± 0.05	1.073	0.512	1.774	± 0.099	1.42	± 0.14	
24 HDS-1820 - MAM	5.91	± 0.31	20	22.28	± 3.87	0.197	± 0.020	0.4891	± 0.209	4.1168	± 0.705	1.4681	± 0.059	1.05	± 0.05	1.211	0.584	1.992	± 0.107	2.97	± 0.22	
25 HDS-1820 - MAM	5.91	± 0.31	20	22.28	± 3.87	0.197	± 0.020	0.5808	± 0.214	3.9092	± 0.723	1.4201	± 0.060	1.05	± 0.05	1.183	0.573	1.953	± 0.106	3.03	± 0.23	1.9533 ± 0.0318
26 HDS-1820 - MAM	5.91	± 0.31	20	22.28	± 3.87	0.197	± 0.020	0.4314	± 0.202	4.2312	± 0.688	1.3928	± 0.059	1.05	± 0.05	1.152	0.566	1.914	± 0.103	3.09	± 0.23	
27 HDS-1821 - MAM	1.93	± 0.17	21	54.67	± 8.58	0.186	± 0.019	0.9839	± 0.205	2.0734	± 0.691	1.3363	± 0.057	1.05	± 0.05	1.131	0.513	1.830	± 0.101	1.05	± 0.11	
28 HDS-1821 - MAM	1.93	± 0.17	21	54.67	± 8.58	0.186	± 0.019	0.8241	± 0.232	2.2974	± 0.790	1.3608	± 0.058	1.05	± 0.05	1.135	0.512	1.832	± 0.105	1.05	± 0.11	1.8635 ± 0.0326
29 HDS-1821 - MAM	1.93	± 0.17	21	54.67	± 8.58	0.186	± 0.019	0.3115	± 0.461	4.3166	± 1.632	1.4113	± 0.084	1.05	± 0.05	1.153	0.561	1.900	± 0.155	1.02	± 0.12	
30 HDS-1821 - MAM	1.93	± 0.17	21	54.67	± 8.58	0.186	± 0.019	0.7224	± 0.203	2.1328	± 0.692	1.4585	± 0.058	1.05	± 0.05	1.190	0.517	1.892	± 0.104	1.02	± 0.11	
31 HDS-1822 - MAM	1.21	± 0.07	113	90.13	± 6.05	0.190	± 0.019	0.8201	± 0.211	3.1957	± 0.704	1.2866	± 0.062	1.05	± 0.05	1.099	0.535	1.824	± 0.103	0.66	± 0.05	1.8728 ± 0.0490
32 HDS-1822 - MAM	1.21	± 0.07	113	90.13	± 6.05	0.190	± 0.019	0.9909	± 0.173	1.8727	± 0.561	1.4402	± 0.063	1.05	± 0.05	1.203	0.529	1.922	± 0.103	0.63	± 0.05	
33 HDS-1823 - MAM	3.49	± 0.34	40	64.56	± 7.29	0.194	± 0.019	0.9971	± 0.215	2.6063	± 0.702	1.2555	± 0.058	1.05	± 0.05	1.086	0.519	1.799	± 0.101	1.94	± 0.22	
34 HDS-1823 - MAM	3.49	± 0.34	40	64.56	± 7.29	0.194	± 0.019	0.7542	± 0.210	3.2552	± 0.697	1.4606	± 0.060	1.05	± 0.05	1.219	0.571	1.985	± 0.107	1.76	± 0.20	1.8919 ± 0.0928
35 All - MAM	1.59	± 0.06		80.35	± 3.74	0.190	± 0.019	0.7522	± 0.215	3.0313	± 0.921	1.3644	± 0.073	1.05	± 0.05	1.144	0.538	1.872	± 0.114	0.85	± 0.06	

References

- Ad-hoc AG Boden: Bodenkundliche Kartieranleitung, 5th ed., Schweizerbart, Hannover, 438 pp., 2005.
- Ad-hoc AG Boden: Bodenkundliche Kartieranleitung, 6th ed., 2 volumes, 552 pp., Schweizerbart, Hannover, 2024.
- Aitken, M. J.: Thermoluminescence dating, Academic Press, London, 359 pp., 1985.
- Aitken, M. J.: An introduction to optical dating: the dating of Quaternary sediments by the use of photon-stimulated luminescence, Oxford University Press, Oxford, 280 pp., <https://doi.org/10.1093/oso/9780198540922.001.0001>, 1998.
- Bøtter-Jensen, L., Bulur, E., Duller, G. A. T., and Murray, A. S.: Advances in luminescence instrument systems, *Radiat. Meas.*, 32, 523–528, [https://doi.org/10.1016/S1350-4487\(00\)00039-1](https://doi.org/10.1016/S1350-4487(00)00039-1), 2000.
- Burow, C.: `calc_CosmicDoseRate()`: Calculate the cosmic dose rate. Function version 0.5.2, in: *Luminescence: Comprehensive Luminescence Dating Data Analysis*. R package version 0.9.21, edited by: Kreutzer, S., Burow, C., Dietze, M., Fuchs, M. C., Schmidt, C., Fischer, M., Friedrich, J., Mercier, N., Philippe, A., Riedesel, S., Autzen, M., Mittelstrass, D., Gray, H. J., Galharret, J., Colombo, M., Steinbuch, L., and de Boer, A., CRAN, <https://doi.org/10.32614/CRAN.package.Luminescence>, 2024.
- DTU Physics: The Risø TL/OSL reader. https://physics.dtu.dk/-/media/institutter/fysik/nutech/produkter-og-services/radiation_measurement_instruments/tl_osl_reader/manuals/reader.pdf, 2021, last access: 26 February 2025.
- Duller, G. A. T.: Distinguishing quartz and feldspar in single grain luminescence measurements, *Radiat. Meas.*, 37, 161–165, [https://doi.org/10.1016/S1350-4487\(02\)00170-1](https://doi.org/10.1016/S1350-4487(02)00170-1), 2003.
- Duller, G. A. T.: The Analyst software package for luminescence data: overview and recent improvements, *Ancient TL*, 33, 35–42, <https://doi.org/10.26034/la.atl.2015.489>, 2015.
- Galbraith, R. F., Roberts, R. G., Laslett, G. M., Yoshida, H., and Olley, J. M.: Optical dating of single grains of quartz from Jinmium rock shelter, northern Australia. Part I: experimental design and statistical models, *Archaeometry*, 41, 339–364, <https://doi.org/10.1111/j.1475-4754.1999.tb00987.x>, 1999.
- Godfrey-Smith, D. I., Huntley, D. J., and Chen, W.-H.: Optical dating studies of quartz and feldspar sediment extracts, *Quat. Sci. Rev.*, 7, 373–380, [https://doi.org/10.1016/0277-3791\(88\)90032-7](https://doi.org/10.1016/0277-3791(88)90032-7), 1988.
- Guérin, G., Mercier, N., and Adamiec, G.: Dose-rate conversion factors: update, *Ancient TL*, 29, 5–8, <https://doi.org/10.26034/la.atl.2011.443>, 2011.
- Kolb, T., Tudyka, K., Kadereit, A., Lomax, J., Poręba, G., Zander, A., Zipf, L., and Fuchs, M.: The μ Dose-system: determination of environmental dose rates by combined alpha and beta counting – performance tests and practical experiences, *Geochronology*, 4, 1–31, <https://doi.org/10.5194/gchron-4-1-2022>, 2022.

Kreutzer, S., Schmidt, C., Fuchs, M. C., Dietze, M., Fischer, M., and Fuchs, M.: Introducing an R package for luminescence dating analysis, *Ancient TL*, 30, 1–8, <https://doi.org/10.26034/la.atl.2012.457>, 2012.

Kreutzer, S.: `fit_LMCurve()`: Nonlinear Least Squares Fit for LM-OSL curves. Function version 0.3.4, in: *Luminescence: Comprehensive Luminescence Dating Data Analysis*. R package version 0.9.21, edited by: Kreutzer, S., Burow, C., Dietze, M., Fuchs, M. C., Schmidt, C., Fischer, M., Friedrich, J., Mercier, N., Philippe, A., Riedesel, S., Autzen, M., Mittelstrass, D., Gray, H. J., Galharret, J., Colombo, M., Steinbuch, L., and de Boer, A., CRAN, <https://doi.org/10.32614/CRAN.package.Luminescence>, 2024.

Li, B., and Li, S. H.: Comparison of De estimates using the fast component and the medium component of quartz OSL, *Radiat. Meas.*, 41, 125–136, <https://doi.org/10.1016/j.radmeas.2005.06.037>, 2006.

Murray, A. S., and Wintle, A. G.: The single aliquot regenerative dose protocol: potential for improvements in reliability, *Radiat. Meas.*, 37, 377–381, [https://doi.org/10.1016/S1350-4487\(03\)00053-2](https://doi.org/10.1016/S1350-4487(03)00053-2), 2003.

Pfaffner, N., Kadereit, A., Kreutzer, S., Kolb, T., Varychev, A., Cionoiu, S., Wang, T., Bertran, P., Bosq, M., Hatté, C., and Sauer, D.: A record of Late Pleistocene environmental conditions at the transition from central to southern Europe from the Baix loess palaeosol sequence (Rhône Rift Valley, SE France), *Quaternary Res.*, (in press).

Tudyka, K., Miłosz, S., Adamiec, G., Bluszcz, A., Poręba, G., Paszkowski, Ł., and Kolarczyk, A.: μ Dose: A compact system for environmental radioactivity and dose rate measurement, *Radiat. Meas.*, 118, 8–13, <https://doi.org/10.1016/j.radmeas.2018.07.016>, 2018.